ADVANCED ELECTRONIC MATERIALS
www.advelectronicmat.de

Trade-Off Between Data Retention and Switching Speed in Resistive Switching ReRAM Devices

Sebastian Siegel, Christoph Baeumer, Alexander Gutsche, Moritz von Witzleben, Rainer Waser, Stephan Menzel, and Regina Dittmann*

Memristive switching devices are promising for future data storage and neuromorphic computing applications to overcome the scaling and power dissipation limits of classical CMOS technology. Many groups have engineered bilayer oxide structures to enhance the switching performance especially in terms of retention and device reliability. Here, introducing retention enhancement oxide layers into the memristive stack is shown to result in a reduction of the switching speed not only by changing the voltage and temperature distribution in the cell, but also by influencing the rate-limiting-step of the switching kinetics. In particular, it is demonstrated that by introducing a retention enhancement layer into resistive switching $SrTiO_3$ devices, the kinetics are no longer determined by the interface exchange reaction between switching oxide and active electrode, but depend on the oxygen ion migration in the additional interface layer. Thus, the oxygen migration barrier in the additional layer determines the switching speed. This trade-off between retention and switching speed is of general importance for rational engineering of memristive devices.

Scaling in integrated circuits is approaching a stalemate, due to the limitations of classical CMOS technology in terms of power dissipation and physical boundaries of geometrical scaling. At the same time, new concepts, such as neuromorphic computing, demand for new functionalities, logic, and data storage approaches. This drives intensive research in new types of electronic devices, so-called memristive devices.[1–8]

As of today, there are multiple types of memristive devices based on different physical concepts. Among those, redox-based resistive switching in transition metal oxide devices plays a prominent role. The fundamental mechanism for the transition between a high resistive state (HRS) and a low resistive state (LRS) in these Redox-based Random Access Memory (ReRAM) cells is a nanoscale redox-reaction due to oxygen-ion migration.[3,9,10–17] During the SET process from the HRS to the LRS, the concentration of oxygen vacancies, which act as donor dopants, is locally increased in the oxide, adding electrons to the conduction band. This reduces the Schottky barrier at the interface to the high work function metal electrode, and results in a lower resistance of the device. The RESET operation, performed with the opposite voltage polarity, decreases the concentration of oxygen vacancies near the interface, increases the Schottky-barrier height or width and thereby increases the resistance.

For many material systems, the SET operation can be performed by applying a negative voltage to the active Schottky-type electrode. It is widely accepted that in this switching mode, positively charged oxygen vacancies in the transition metal oxide layer are attracted toward the negatively biased electrode, thereby increasing their concentration near the interface. In turn, the oxygen vacancies are repelled upon application of a positive voltage in the RESET operation, decreasing the interface concentration. This thoroughly-studied type of switching, also called "counter-eightwise switching" is due to purely internal redistribution of oxygen vacancies.[1,4,18]

However, for many material systems, such as TiO_{2-x},[19,20] HfO_{2-x},[21,22] Ta_2O_{5-x},[23,24] and $SrTiO_3$,[25,26] it has been reported that it is also possible to switch the devices with the opposite set of voltage polarities, more precisely, to perform the SET with a positive voltage to the active Schottky-type electrode, and the RESET with a negative voltage. This is called anomalous or "eightwise switching." One interesting feature of this switching mode is the gradual switching capability in both SET and RESET directions, which makes it very promising for analog≈ and neuromorphic computing.[27–30] The anomalous switching process cannot be explained by the model of purely internal redistribution of oxygen vacancies. It has been shown that the mechanism for this switching mode works via an interface exchange reaction of oxygen at the active interface electrode in combination with ion movement in the bulk.[9,20,24,31]

S. Siegel, Dr. C. Baeumer, A. Gutsche, Prof. Dr. R. Waser, Dr. S. Menzel, Prof. Dr. R. Dittmann
Peter Grünberg Institut (PGI-7 / 10)
Forschungszentrum Jülich GmbH & JARA-FIT
Jülich 52425, Germany
E-mail: s.siegel@fz-juelich.de

Dr. C. Baeumer, M. von Witzleben, Prof. Dr. R. Waser
Institute of Electronic Materials (IWE2) & JARA-FIT
RWTH Aachen University
Aachen 52074, Germany

The ORCID identification number(s) for the author(s) of this article can be found under https://doi.org/10.1002/aelm.202000815.

DOI: 10.1002/aelm.202000815

The strong role of the active interface allows for drastically increasing the retention of inscribed states by interface engineering with additional oxide layers having a low oxygen mobility, as we demonstrated by comparing $SrTiO_3$ cells with direct platinum interface to cells with interfacial SrO and Al_2O_3 layers.[32] But so far it remains unclear how this kind of interface engineering influences the switching kinetics. Such additional oxide interlayers in redox-based RRAM devices have been proposed in manifold ways.[33–36] Therefore, this question is highly relevant for rational engineering of redox-based resistive switching devices.

In this work, we will investigate the switching kinetics of the eightwise-switching process in the model system of $SrTiO_3$-based ReRAM cells. We will identify the rate-determining step (RDS) of the switching kinetics in the oxygen-release during the SET process by modeling the underlying physical processes and comparing calculated with measured kinetics. Furthermore, we investigate samples with interface oxide layers exhibiting slow oxygen migration and investigate their impact on the rate-limiting step and the switching kinetics.

We compare the SET switching kinetics of $SrTiO_3$-based ReRAM cells with different material stacks. The 10 nm thick $SrTiO_3$ thin films are grown epitaxially on single-crystalline niobium-doped $SrTiO_3$ substrates by Pulsed Laser Deposition (PLD). For two kinds of ReRAM cells, the $SrTiO_3$ layer is stoichiometric (Sr:Ti ratio 50:50), while for one type of device the $SrTiO_3$ is grown to be Sr-rich (Sr:Ti ratio ≈52/48). The latter layer exhibits a SrO terminating layer on the surface of the $SrTiO_3$ thin film.[37,38] Onto one of the stoichiometric $SrTiO_3$ layers, a 1 nm thick layer of Al_2O_3 is deposited by PLD. Finally, all samples are covered by micrometer-sized patterned platinum top electrode, yielding one type of device with stoichiometric $SrTiO_3$ and a direct interface to the platinum top electrode, one with Sr-rich $SrTiO_3$ and a SrO interface layer and one with stoichiometric $SrTiO_3$ and an Al_2O_3 interface layer. The Nb:$SrTiO_3$ substrate is used as the grounded bottom electrode and the voltage is applied to the platinum top electrode. It should be noted that at the edge of the top electrode, a triple-phase boundary exists between the top oxide layer ($SrTiO_3$ or the interlayer material), platinum, and air.

Initially, the devices are formed with a quasi-static voltage sweep to +3 V (sweep rate 650 mV s^{-1}). The current in this forming step is limited to 30 mA. In preparation for stable and reproducible switching kinetics measurements, the cells are switched between the LRS (ON state) and the HRS (OFF state) multiple times with voltage sweeps between +2 V and −3 V (sweep rate of 650 mV s^{-1} for both) with a current compliance of 10 mA in the positive SET direction. More details can be found in the Experimental Section and the Supporting Information.

To measure the SET switching kinetics, negative voltage pulses are used to reset the cells to a defined high resistive OFF state (HRS) of 2.5 MΩ ± 15%, before applying a positive voltage pulse of defined length and height. The resistance of the cell is read before and after each pulse by read-out pulses of 0.3 V for 60 ms (see **Figure 1**a). Both read measurements are compared to obtain the resulting OFF-ON-ratio $\frac{R_{OFF}}{R_{ON}}$. For each voltage in the measurement range, the pulse length of the SET pulse is increased until the OFF–ON ratio overcomes the value of 10, indicating that the cell has switched. The relation between

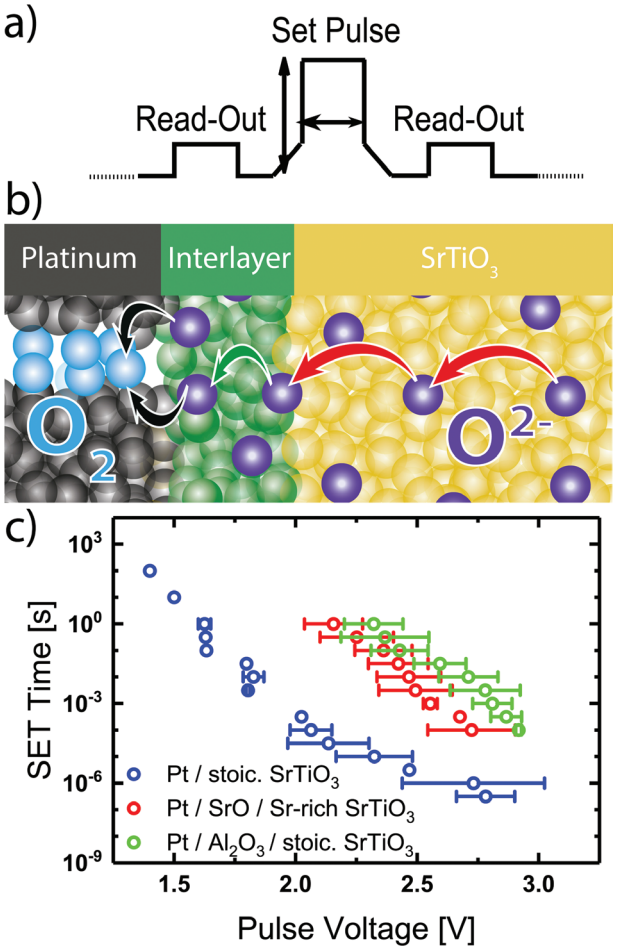

Figure 1. a) Pulse scheme for switching kinetics measurement. Before and after the actual pulse voltage, the read voltage is applied. b) Assumed processes taking place in the oxygen release process: red arrow: oxygen ion migration in the $SrTiO_3$; green arrow: oxygen ion migration in the interlayer (if applicable); black arrows: interface exchange reaction. c) Comparison of measured switching kinetics for different material stacks.

switching voltage and switching time represents the switching kinetics and is displayed in Figure 1c. In this study, the switching time is defined as the pulse length necessary to cause an OFF-ON-ratio of 10. A sharp switching event like in other studies investigating the switching kinetics cannot be observed, due to the convergence of HRS and LRS for high voltages (only one IV relation can be seen in Figure S2, Supporting Information). The switching kinetics of the stoichiometric $SrTiO_3$ layer with direct Pt interface are shown in blue. Between 1.4 V, where it takes a pulse of about 100 s to switch the cell, to 2.1 V and a switching time of 100 µs, the slope of the switching times in the logarithmic plot is constant at 100 mV $dec.^{-1}$ For higher voltages, the slope decreases to about 350 mV dec^{-1}.

Interface engineering with additional oxide layers has a significant influence on the switching kinetics (see Figure 1c) red and green). At about 2.3 V, cells with a SrO (Al_2O_3) interlayer need four (five) orders of magnitude longer pulses to switch than cells with a direct $SrTiO_3$/platinum interface. In the measured range, the slopes of the switching kinetics (140 mV/dec^{-1} and 150 mV dec^{-1} for the Sr-rich sample with SrO and the

Al_2O_3 interlayer sample, respectively) are lower for the cells with interface engineering than for the cells without.

One can imagine two possible reasons for the differences in the shape and the slope of the switching kinetics of the different material stacks. The first possible reason is that the power and voltage applied to the cells are different. Temperature and voltage distribution in the cell can have a major influence on the switching kinetics.[39–42] Furthermore, different material parameters like diffusion constants can have a severe effect on the switching speed. The second possibility is that for each cell type, with and without interface engineering, different processes are rate-determining.[43] To clarify the origin of the different switching kinetics, models for the switching kinetics determined by different possible processes are obtained and the temperature and voltage distribution of the different cells are simulated with a finite element method (FEM) in a model proposed by Menzel et al.[40]

Based on our previous studies, the eightwise switching mechanism in these cells occurs via a release and reincorporation of oxygen from the $SrTiO_3$ layer.[9,31] This oxygen exchange process consists of different intermediate steps. Two can be considered as possibly rate-limiting and are depicted in Figure 1b: The first step is the movement of oxygen ions through the oxide toward the platinum interface (red and green arrows) and the second step the release from the $SrTiO_3$ at this very interface (black arrows). This is assumed to happen in an interface-exchange reaction, where oxygen ions are extracted from the $SrTiO_3$ and evolve as molecular oxygen O_2. Due to the triple-phase boundary at the edge of the top oxide layer, it is not exactly clear, if the oxygen is transferred from the top oxide layer into the platinum layer or the ambient air. But even at the triple-phase boundary, the presence of the platinum layer would already significantly lower the energy barrier for the interface exchange reaction.[44] Both processes, however, can be described with Butler-Volmer kinetics as stated below. In a previous study, we could avoid such triple-phase boundary and showed that oxygen also transfers into the platinum layer, because switching could be maintained for multiple cycles even in reducing atmospheres.[30] The evolution process of O_2 involves the transfer of four electrons and various intermediate steps.[44] The steps of the exchange reaction are, in Kröger–Vink notation:

$$O^{X}_{O} \Leftrightarrow O' + e' + V_o^{\cdot\cdot} \tag{1}$$

$$2\,O' \Leftrightarrow O_2'' \tag{2}$$

$$O_2'' \Leftrightarrow O_2' + e' \tag{3}$$

$$O_2' + \dot{h} \Leftrightarrow O_2 \tag{4}$$

according to Merkle et al.[44] and equations (2) and (3) were determined to be rate-determining for the interface exchange reaction.[45] Following the work of Bockris et al.[46] and Noren et al.,[47] one can now determine the reaction coefficients up to a fitting parameter $\beta \in [0,1]$ to

$$\alpha_{red} = 1 - \beta \text{ and } \alpha_{ox} = 1 + \beta. \tag{5}$$

A model for the switching kinetics based on this interface-exchange reaction can be obtained from the Butler–Volmer equation,

$$j_{Exchange} = j\left(e^{\alpha_{red}\frac{e}{k_B T}\Delta V_{act}} - e^{-\alpha_{ox}\frac{e}{k_B T}\Delta V_{act}} \right) \text{ with } \Delta V_{act} = V_{act} - V_{interface} \tag{6}$$

with the Boltzmann constant k_B, the average interface temperature T, the activation and interface potential V_{act} and $V_{interface}$, which describe the electric current density $j_{Exchange}$ across the interface upon applying an effective interface potential ΔV_{act} from an imbalance between the reduction and oxidation process at the interface, given by the exponential terms. Here, the Butler–Volmer equation is used to describe the amount of oxygen involved in the oxygen release and oxygen incorporation reaction. From XPEEM measurements, we previously determined that about 4 at% of oxygen ions are removed from the switching oxide in $SrTiO_3$-based devices in similar switching experiments.[48] The major increase of oxygen vacancy concentration occurs within some nanometers below the active electrode, as we could show by in situ transmission electron microscopy.[9] Hence, we assume that on average oxygen is released from within a depth of 1 nm within the lattice.

Each release of an oxygen ion leads to a transfer of two electrons. This allows for calculating the area charge density, which is transferred during the SET process q_{redox} to

$$q_{redox} = 1.8\frac{C}{m^2} \tag{7}$$

A detailed derivation of this value is provided in the Supporting Information. One can now define the switching time as this charge density, divided by the exchange current $j_{exchange}$ resulting from the exchange reaction:

$$\Delta t_{SET} = \frac{q_{redox}}{j_{Exchange}} \tag{8}$$

When assuming the equilibrium exchange current to be temperature-dependent and following an Arrhenius' Law, with the activation energy ΔW_e and a prefactor j_0, as

$$j = j_0\, e^{-\frac{\Delta W_e}{k_B T}} \tag{9}$$

and introducing the calculated exchange coefficients (equation (5)), the formula for the switching time (equation (10)) can be re-written as

$$\Delta t_{SET} = \frac{q_{redox}}{2\, j_0}\, e^{\frac{\Delta W_e + \beta e \Delta V_{act}}{k_B T}} \left(\sinh\left(\frac{e}{k_B T}\Delta V_{act} \right) \right)^{-1} \tag{10}$$

The second process involved in the anomalous switching is the migration of oxygen ions toward the interface. If this process is the RDS, the SET kinetics can be described using the Mott–Gurney law (or, more precisely, by the Genreith–Schriever–DeSouza law[49]) and defining the SET time as the time, when the charge, which is moved during a SET process,

as calculated above, has been moved.[43] The SET time can then be written as

$$\Delta t_{\mathrm{SET}} = \frac{q_{\mathrm{redox}}}{j_{\mathrm{ion\ motion}}} \tag{11}$$

with the electric current density resulting from the ion motion $j_{\mathrm{ion\ motion}}$. Following the work of Menzel et al.,[50] this current density can be obtained from the Mott–Gurney law, resulting in

$$\Delta t_{\mathrm{SET}} = \frac{q_{\mathrm{redox}}}{2\ z\ a_{\mathrm{cell}}\ c_{\mathrm{O}}\ f_{\mathrm{a}}} e^{\frac{\Delta W_{\mathrm{m}}}{k_{\mathrm{B}}T}} \left(\sinh\left(\frac{eaE}{k_{\mathrm{B}}T}\right)\right)^{-1} \tag{12}$$

as the SET time, where $z = 2$ is the charge number of the oxygen ions, a_{cell} the unit cell size of the material the ions are moving in, c_{O} the concentration of oxygen ions in the material and f_{a} the jump attempt frequency. ΔW_{m} is the energy barrier for the ion migration.

Comparing the formulas for the SET kinetics, one can see that the overall structure is the same with a hyperbolic sine term in the end and an Arrhenius-like term in the beginning. The major difference is that in the Butler-Volmer-Model (equation (10)) for the SET kinetics limited by the interface exchange reaction, the exponential in the Arrhenius term has a voltage component and is therefore depending on the electric field.

Now, after obtaining formulas for the switching times with either assuming (1) the interface exchange reaction (equation (10)) or (equation (2)) the ion movement toward the interface (equation (12)) to be rate-limiting, we can calculate the theoretical switching kinetics and compare the results to measured switching kinetics. Both formulas require information about the temperature and electric field in the cell and at the interface. Values for the electric field, potential, and temperature terms in equations (equation (10)) and (equation (12)) are obtained from FEM simulations with the commercial software COMSOL Multiphysics (see Supporting Information). The simulated geometry resembles the fabricated cells assuming a filament radius of 300 nm, similar to simulations by Menzel et al.[40] and comparable to the area of valence change in our XPEEM measurements of switched devices.[32] For the ion motion in (equation (12)) in the $SrTiO_3$, the average field and temperature values from a 1 nm region below the interface ("diode") to the top layer in the filament radius are used. Similarly, the ion motion in the interlayer uses the same values acquired from the oxide interlayer region on top of the $SrTiO_3$. For the interface exchange reaction (equation (10)) the average temperature and electric field data in the region of the assumed filament radius at the interface between the platinum and its lower region is used.

The results for the expected SET kinetics for each device geometry based on (equation (10)) and (equation (12)) are shown in **Figure 2** and compared to the experimental data. When calculating the switching kinetics depending on ion migration with the Mott–Gurney model (equation (12)) and comparing it to the measured switching kinetics of cells with stoichiometric $SrTiO_3$ with a direct interface to the platinum electrode, it becomes apparent that for the anomalous switching mode investigated here, the ion motion in the $SrTiO_3$ layer is not the RDS, because the calculated switching times (see red line in Figure 2a) are

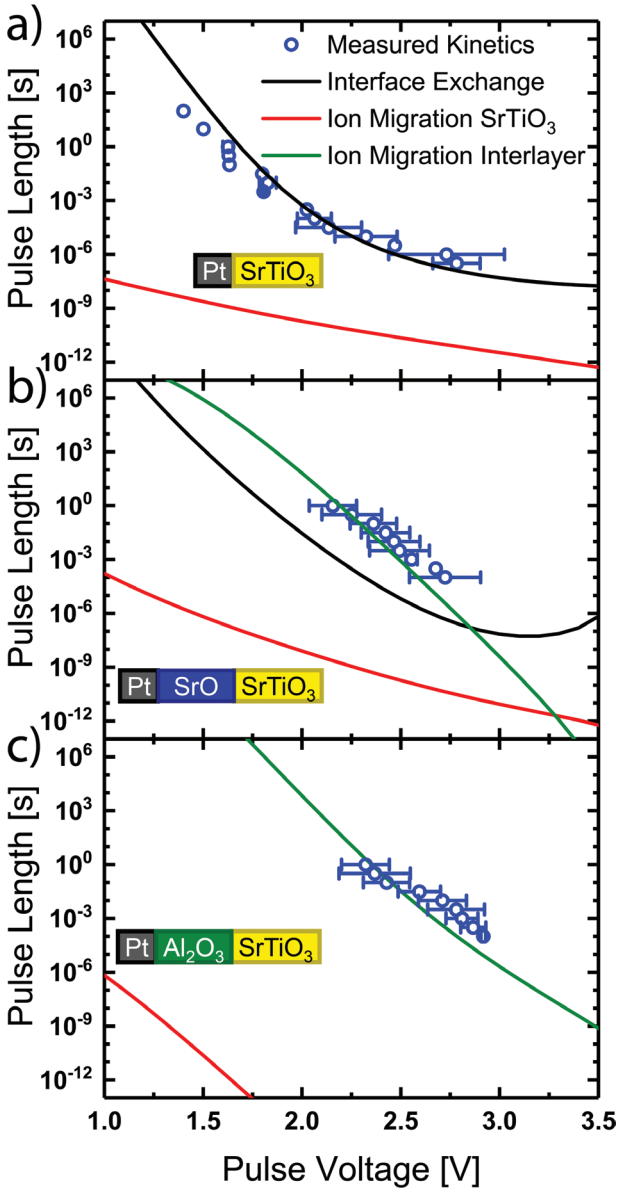

Figure 2. The relation between pulse voltage and length that is necessary to achieve a certain ON–OFF ratio is the switching kinetics. Simulated switching kinetics in comparison to measured switching kinetics. a) For devices with a direct interface between the switching $SrTiO_3$ and the active electrode, the interface exchange reaction is rate-limiting. b) When introducing a SrO interlayer, the ion migration in this interlayer becomes rate-limiting. c) Also for an Al_2O_3 interlayer, the oxygen ion migration in the interlayer is rate-limiting.

orders of magnitude faster than the measured switching times. In contrast, these switching times can be fitted closely with the Butler–Volmer model (equation (10)) for the interface exchange reaction as the RDS (black line in Figure 2a), choosing the parameters displayed in **Table 1**. Where references are given, the values in this table are taken from the literature. Otherwise, they are fitted to match the measured current-voltage-characteristics (see Figure S2, Supporting Information). The fitted value for the equilibrium exchange current density j_0 is in the range of typical values for mixed conducting perovskites.[51,52]

Table 1. Parameters for the Butler–Volmer model for the switching kinetics depending on the oxygen interface exchange reaction. Values for the equilibrium exchange current $j_{0,0}$, asymmetry factor β, and overpotential Φ_0 are fitted parameters. The activation energy for the SrO/Pt interface device is assumed equal to the one of the $SrTiO_3$/Pt interface device, because to the author's best knowledge, no value has been determined yet.

	$SrTiO_3$/Pt	SrO/Pt	Al_2O_3/Pt
$j_{0,0\vert}$ [Am^{-2}]	2×10^2	2×10^2	$10^{38a)}$
ΔW_E [eV]	1.3[64]	1.3	6.7[65]
Φ_0 [V]	0.35	0.35	0.35
β [1]	0.1	0.1	0.1

[a)] (Physically unrealistic value compared to equilibrium exchange currents from the literature [51,52] only used for the sake of showing the numerically closest possible fit);

In principle, one could also consider the oxygen diffusion in the platinum top electrode as a possible rate-limiting step. Oxygen is released from the $SrTiO_3$ layer to the interface with the platinum top electrode. This could also lead to a rate-limitation, when released oxygen accumulates at the interface and occupies all available sites, thereby hindering further oxygen from being released. The very low diffusion coefficient of oxygen in bulk platinum could support this argument. But measured diffusion coefficients, especially for defect-rich platinum, exhibit significantly higher values. Since the platinum in our cells is deposited by thermal evaporation, it can be expected that it is defect-rich. The higher diffusion coefficients are due to multiple factors such as enhanced diffusion along grain boundaries[53,54] and fast surface diffusion,[55] especially along step edges.[56] Therefore, taking the value of the oxygen diffusion coefficient given by Velho et al., which is $2.5*10^{-9}$cm s^{-1} at room temperature,[57] the time oxygen needs to diffuse 1 nm away from the surface (which is about three times the lattice constant of platinum) can be estimated using.[58]

$$t \approx \frac{\langle x^2 \rangle}{2\ D} \tag{13}$$

with the mean-square displacement of the oxygen atoms $\langle x^2 \rangle$ and the diffusion coefficient D and to about 2 µs. The diffusion coefficient is temperature-activated. Therefore, this is a conservative estimate and still much faster than the measured and calculated switching time for lower voltages. At about 3 V, the switching times approach the µs regime, but at the same time, the interface temperature increases. This leads to an enhanced diffusion and speeds up the diffusion time for movement within the platinum electrode to about 50 ns, which is again faster than the measured switching kinetics. Therefore, the diffusion of oxygen in the platinum electrode is not considered as a possible rate-limiting step in this study. Therefore, we suggest that the RDS for this type of cell in the anomalous switching mode is the exchange reaction of oxygen at the $SrTiO_3$–platinum interface.

On the other hand, for the cells with an additional interfacial oxide layer, the switching kinetics cannot be modeled with the Butler–Volmer model (12) for the interface exchange. The calculated kinetics based on the fitting to the *I–V* characteristics do not fit the measured switching time values (black line in Figure 2b). For the Al_2O_3-interlayer cells the calculated switching kinetics, when dependent on the interface exchange, can approach the measurement values, when using a physically unreasonably high equilibrium exchange current of 10^{38} Am^{-2}. This is not only much higher than the equilibrium exchange current used for the other two cell types of $2*10^2$ Am^{-2}, but also orders of magnitude higher than values found in the literature.[51,52] Furthermore, the oxygen ion motion in the $SrTiO_3$ layer (red lines) cannot be the rate-limiting step for the switching kinetics, similar to the case for the $SrTiO_3$/Pt interface. Actually, for cells with an additional oxide interlayer, the measured switching kinetics are close to the calculated kinetics limited by the ion motion in the additional oxide interlayer (green lines), using the literature values given in **Table 2**. Therefore, we suggest the ion motion in the oxide interlayer as the RDS of the switching kinetics of ReRAM cells with an additional interfacial oxide layer. While a different RDS explains the large difference in switching times between devices with and without an interfacial oxide layer, also the interlayer material plays an important role in the switching speed. As one can see in Figure 1c, devices with an Al_2O_3 interlayer switch one order of magnitude slower than those with a SrO interlayer. According to the simulations carried out here, for both device types the oxygen ion migration is the RDS of the switching kinetics. However, the activation energy for this motion is 0.2 eV higher for defect-rich Al_2O_3 with 1.8 eV[59] than for SrO([32]).

Table 2. Parameters for the Mott–Gurney model for the switching kinetics depending on the oxygen ion migration. Attempt frequencies assumed from Menzel et al.[43]

	$SrTiO_3$	SrO	Al_2O_3
ΔW_M [eV]	1.01[66]	1.6[32]	1.8[67,59]
f_a [Hz]	10^{13}	10^{13}	10^{13}
a_{cell} [Å]	3.905[68]	5.1[69]	4.8[70]

While these differences in the material stacks and material parameters give a consistent explanation for the different switching kinetics, it is still possible that the voltage and/or temperature distribution in the different device stacks is largely different and that actually this governs the switching speed. In the following, we will show that this is not the case as there is no major difference in the electrical power dissipation in the cells and it is solely the presence of the additional oxide interlayer which changes the RDS of the switching kinetics. This is illustrated in an exemplary comparison between the cells with no interlayer and the cells with an alumina interface layer (**Figure 3**). The voltage applied to the device is divided between the voltage drops over the Schottky barrier within the $SrTiO_3$ layer at the interface, the interface oxide layer, and the bulk part of the $SrTiO_3$. Figure 3a displays the voltages in the different parts of the stack and the oxygen ion migration barrier as a function of applied voltage. Figure 3b sketches the path oxygen ions have to pass to be released at the interface and indicates the potential barriers for the ion migration in the materials and

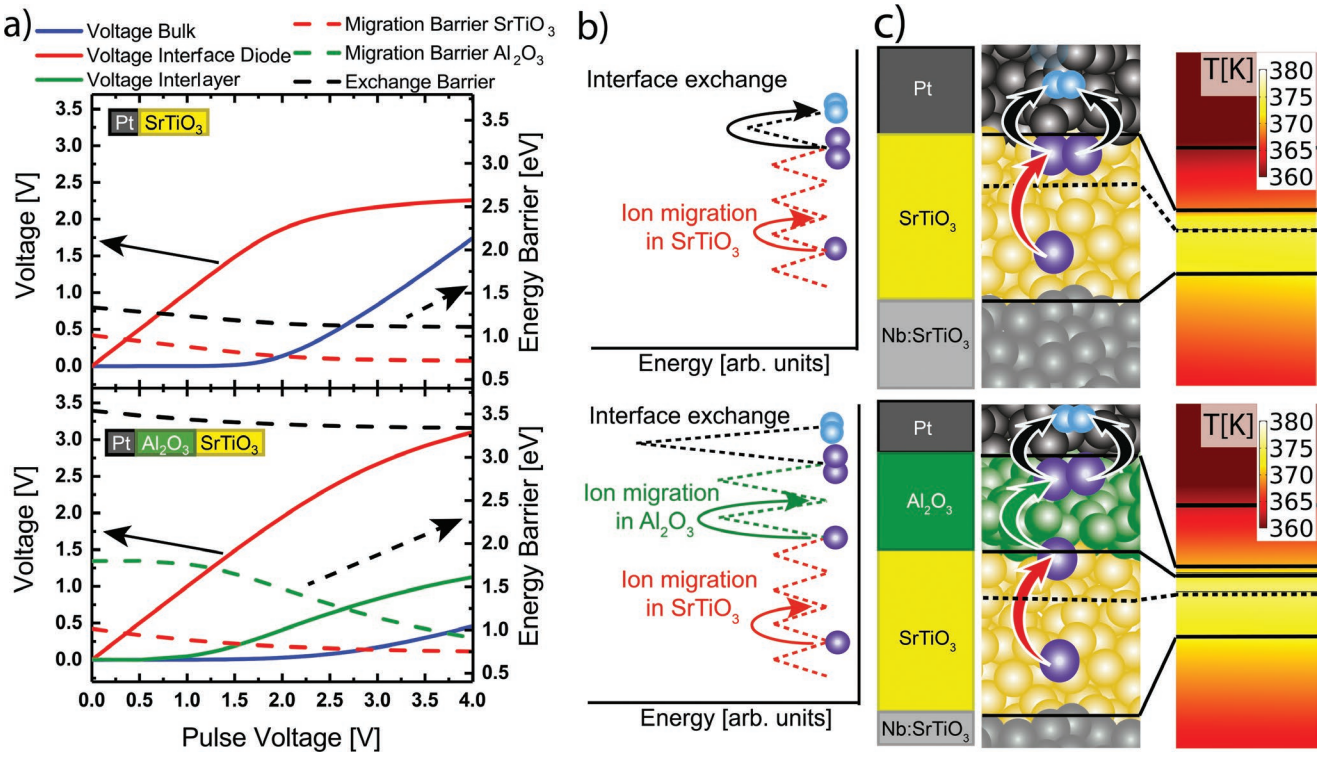

Figure 3. a) Evolution of voltage distribution and process energy barriers. Solid lines show the voltages dropping over the respective areas of the memristive stack. Dashed lines give the activation barriers of the indicated processes; b) Sketched energy barriers on the complete pathway to oxygen release. Arrows indicate the relevant processes, which can be found in the sketch to the right; c) Relevant processes for oxygen removal: Oxygen ion (violet) migration in $SrTiO_3$ (red arrow) and the interlayer (green, if applicable) and interface exchange reaction (black arrows). Sketch of temperature distribution for a 3 V pulse (lines show boundaries of different material layers)

the exchange reaction at the interface. For both cells at low voltages, voltage mostly drops across the interfacial Schottky barrier (red solid line). With increasing voltage, the voltage drop across the Schottky barrier increases further, which causes a decrease of the oxygen ion migration barrier in the $SrTiO_3$ and a decrease of the interface exchange barrier for the cell without an interlayer. The decreased oxygen ion migration barrier can be obtained from the Mott–Gurney law as $\Delta W_m - \frac{eaE}{k_B T}$, which is used to obtain equation (equation (12)). The decreased interface exchange barrier originates from the Butler–Volmer model (equation (10)) as $\Delta W_e + \beta e \Delta V_{act}$. For the cell with a direct $SrTiO_3$ interface to platinum, the slope of the voltage drop over the interfacial Schottky barrier decreases for voltages above 2 V, as the voltage increasingly drops over the $SrTiO_3$ series resistance. The ion migration and interface exchange barriers are not lowered further (black and red dashed lines in Figure 3a) and the switching kinetics flatten (compare Figure 2a). For the cell with an Al_2O_3 interlayer, on the other hand, less voltage drops over the $SrTiO_3$ far away from the interface but instead over the interlayer (green solid line in Figure 3a). This leads to a steady decrease of the ion migration barrier in this interface layer (green dashed line) and goes together with the continuously decreasing switching times in the switching kinetics of this cell type (compare Figure 2c). The energy barrier for the interface exchange reaction in the cells with an Al_2O_3 interlayer is much higher than the migration barriers in the $SrTiO_3$ and the Al_2O_3 layer. But since it is sufficient that the oxygen is released from the $SrTiO_3$ into the Al_2O_3, this process is not important for the switching process and plays no role for the switching kinetics.

Importantly, it is actually the voltage modulation of the potential barrier governing the RDS of each cell that shapes the switching kinetics. Moreover, the temperature distribution is similar between cells with and without an Al_2O_3 interlayer in the voltage region, where the switching kinetics are measured. This is shown for the example of 3 V applied voltage in Figure 3c. Therefore, the switching speed depends merely on the voltage modulation of the different RDS and is neither caused by major differences in the temperature distribution, nor due to a largely different voltage division in the cell.

In conclusion, we have shown that the switching kinetics of $SrTiO_3$-based anomalous resistive switching cells can be influenced heavily by engineering the interface between the $SrTiO_3$ and the active high work function metal electrode. A direct interface between these two layers leads to comparably fast switching, while additional interfacial oxide layers drastically decrease the switching speed. This is not due to different dissipation of electrical power or major differences in the distribution of the applied voltage, but to a change in the rate-determining step of the oxygen release process that determines the switching kinetics. For cells with no interfacial oxide layer, we showed that this RDS is the interface exchange reaction of oxygen, while for the cells with an interlayer, the ion movement in the interlayer material becomes rate-limiting. In that case, the material parameters of the interlayer become crucial for the

switching speed and higher migration barriers cause slower switching.

This result has important consequences for rational design of resistive switching devices. Depending on the purpose of the memristive device, a different approach for optimization must be chosen. While dedicated memory elements demand for long data retention, computational memory might emphasize high switching speed. As was shown in previous works, the introduction of interfacial oxygen layer increases the retention of the devices drastically,[32,60] but on the other hand, like in this study, it slows down the switching speed. This decrease in switching speed could be possibly mitigated by choosing a material with a low oxygen migration barrier as the interface layer. For devices without an oxide interface layer, an enhancement of the surface electrons could increase the switching speed. Of course, this would on the other hand decrease the retention of the device. The interest in bi- and mult-ilayer devices has increased drastically over the last years, due to the often superior retention and stability of these devices.[61–63] In this study, we showed that this kind of cell design, on the other hand, can have large influence on the switching speed. This is an important trade-off between state retention and switching speed, which is crucial for rational device engineering.

Experimental Section

Device Preparation: Device Fabrication: 10 nm of (stoichiometric/Sr-rich) $SrTiO_3$ were deposited onto 0.5 at%-doped $SrTiO_3$ substrates manufactured by Crystec GmbH (Germany) with a (100)-oriented surface. Prior to deposition, the substrates were annealed in air for 4 h at 950 °C. The deposition was carried out by Pulsed Laser Deposition (PLD) with a KrF excimer laser (λ = 248 nm) with a laser fluence of 1.5 J cm^{-2} for stoichiometric films and 1 J cm^{-2} for Sr-rich films with a repetition rate of 5 Hz at a substrate temperature of 800 °C and an oxygen partial pressure of 0.1 mbar.

An Al_2O_3 film of 1 nm thickness was deposited ex situ with PLD with a laser fluence of 2.1 J cm^{-2} and a repetition rate of 5 Hz in an oxygen atmosphere of 10^{-4} mbar at room temperature. Since Al_2O_3 was dissolved by the developer for the optical lithography, Microchemical's AZ MIF 326, for this sample, a 10 nm platinum protective layer was deposited onto the Al_2O_3 layer which then can be structured to contact pads with equal size as for the other material stacks investigated by optical lithography and ion beam etching.

For all samples, an 80 nm thick insulating oxide layer was deposited and patterned by optical lithography to open contact holes to the $SrTiO_3$ or Al_2O_3 layer. (see Supporting Information for details on the cell geometry). The metal contacts were fabricated by depositing electron-beam evaporation of 10 nm platinum followed by 80 nm of gold and patterned by optical lithography and a lift-off process. The size of each device was 3 µm x 9 µm and the contact area separated from the active layer by the thick insulating oxide was 250 µm × 140 µm. A sketch of the device geometry was given in Figure S3, Supporting Information. The additional insulating oxide layer plays no role in the switching process. It was used to separate the actual device from the contact area, where the device was contacted with a probe station. On the one hand, it acts as a mechanical protection of the $SrTiO_3$ layer from being punched through by the contact needle, which would shorten the device. On the other hand, it allows for large contact areas compared to the device size without drastically increasing the capacity of the device. This would lead to long *RC*-times and make it impossible to appropriately measure short pulse length. By this means the *RC*-times were kept at least two orders of magnitude below the measured switching kinetics.

SET Kinetics Measurement Procedure: The SET switching kinetics were measured by applying a voltage pulse of increasing length (100 ns to 1 s in half logarithmic steps) and height (1 to 3.5 V in steps of 0.25 V). For pulses shorter than 1 µs, the rise and fall times were 100 ns while for pulses longer than 1 ms they were 1 µs. For all other pulses, the rise and fall times were 10% of the respective pulse length each. Prior to the rise to the actual pulse voltage, the voltage was increased in a 1 ms ramp to the read voltage of 0.3 V. This leads to more reproducible switching kinetics measurements. All voltages were applied with respect to the active electrode while the ohmic electrode was always grounded. The resistances before and after the potential SET pulse was measured with a 60 ms pulse of 0.3 V and the resistance calculated as the quotient of the current and the applied voltage. If the ratio of the resistance before and after the voltage pulse was greater or equal to 10, this was defined as a switching event. In order to provide a comparable measurement procedure, prior to the application of a SET pulse, the cell was transformed into a defined HRS of 2.5 MΩ +- 15%. Negative RESET pulses of 1 ms length and increasing height or positive pulses of 2.5 V and 100 µs length were applied, if the cell's resistance was below of below or above this value, respectively.

Supporting Information

Supporting Information is available from the Wiley Online Library or from the author.

Acknowledgements

This work was supported by the DFG (German Science Foundation) within the collaborative research center SFB 917 "Nanoswitches" and by the Helmholtz Association Initiative and Networking Fund under project number SO-092 (Advanced Computing Architectures, ACA) and the Federal Ministry of Education and Research (project NEUROTEC grant no. 16ES1133K). CB received funding from the European Union's Horizon 2020 research and innovation programme under the Marie Sklodowska-Curie grant agreement No 796142. The authors gratefully acknowledge fruitful discussions on oxygen movement in platinum with A. Zurhelle (IWE2, RWTH Aachen University) and J. Dederichs for cross-checking of the manuscript.

Open access funding enabled and organized by Projekt DEAL.

Conflict of Interest

The authors declare no conflict of interest.

Keywords

bilayer ReRAM cells, device engineering, ReRAM, switching kinetics

Received: August 13, 2020
Revised: September 16, 2020
Published online: November 30, 2020

[1] R. Waser, R. Bruchhaus, S. Menzel, *Redox-Based Resistive Random Access Memories*, **2012**.
[2] D. B. Strukov, G. S. Snider, D. R. Stewart, R. S. Williams, *Nature* **2008**, *453*, 80.
[3] R. Waser, M. Aono, *Nat. Mater.* **2007**, *6*, 833.
[4] J. J. Yang, M. D. Pickett, X. Li, D. A. A. Ohlberg, D. R. Stewart, R. S. Williams, *Nat. Nanotechnol.* **2008**, *3*, 429.

[5] H. S. P. Wong, L. Heng-Yuan, Y. Shimeng, C. Yu-Sheng, W. Yi, C. Pang-Shiu, L. Byoungil, F. T. Chen, T. Ming-Jinn, *Proc. IEEE* **2012**, *100*, 1951.
[6] X. Hong, D. J. Loy, P. A. Dananjaya, F. Tan, C. Ng, W. Lew, *J. Mater. Sci.* **2018**, *53*, 8720.
[7] T. Chang, K. Chang, T. Tsai, T. Chu, S. M. Sze, *Mater. Today* **2016**, *19*, 254.
[8] R. Yang, H.-M. Huang: Q.H. Hong, X.-B. Yin, Z.-H. Tan, T. Shi, Y.-X. Zhou, X.-S. Miao, X.-P. Wang, S.-B. Mi, C.-L. Jia, X. Guo, *Adv. Funct. Mater.* **2017**, *28*, 1704455.
[9] D. Cooper, C. Baeumer, N. Bernier, A. Marchewka, C. La Torre, R. E. Dunin-Borkowski, S. Menzel, R. Waser, R. Dittmann, *Adv. Mater.* **2017**, *29*, 1700212.
[10] C. Lenser, M. Patt, S. Menzel, A. Köhl, C. Wiemann, C. M. Schneider, R. Waser, R. Dittmann, *Adv. Funct. Mater.* **2014**, *24*, 4466.
[11] A. Koehl, H. Wasmund, A. Herpers, P. Guttmann, S. Werner, K. Henzler, H. Du, J. Mayer, R. Waser, R. Dittmann, *APL Mater.* **2013**, *1*, 042102.
[12] M. Janousch, G. I. Meijer, U. Staub, B. Delley, S. F. Karg, B. P. Andreasson, *Adv. Mater.* **2007**, *19*, 2232.
[13] K. Skaja, C. Bäumer, O. Peters, S. Menzel, M. Moors, H. Du, M. Bornhöfft, C. Schmitz, C.-L. Jia, C. M. Schneider, J. Mayer, R. Waser, R. Dittmann, *Adv. Funct. Mater.* **2015**, *25*, 7154.
[14] Z. Wei, Y. Kanzawa, K. Arita, Y. Katoh, K. Kawai, S. Muraoka, S. Mitani, S. Fujii, K. Katayama, M. Iijima, T. Mikawa, T. Ninomiya, R. Miyanaga, Y. Kawashima, K. Tsuji, A. Himeno, T. Okada, R. Azuma, K. Shimakawa, H. Sugaya, T. Takagi, R. Yasuhara, H. Horiba, H. Kumigashira, M. Oshima, *IEEE Tech. Dig.* **2008**, 293.
[15] Y. Yang, S. Choi, W. Lu, *Nano Lett.* **2013**, *13*, 2908.
[16] G.-S. Park, Y.-B. Kim, S. Y. Park, X. S. Li, S. Heo, M. J. Lee, M. Chang, J. H. Kwon, M. Kim, U.-I.n Chung, R. Dittmann, R. Waser, K. Kim, *Nat. Commun.* **2013**, *4*, 2382.
[17] T. Bertaud, M. Sowinska, D. Walczyk, S. Thiess, A. Gloskovskii, C. Walczyk, T. Schroeder, *Appl. Phys. Lett.* **2012**, *101*, 143501.
[18] R. Waser, R. Dittmann, G. Staikov, K. Szot, *Adv. Mater.* **2009**, *21*, 2632.
[19] F. Miao, J. J. H. Yang, J. Borghetti, G. Medeiros-Ribeiro, R. S. Williams, *Nanotechnology* **2011**, *22*, 254007.
[20] H. Zhang, S. Yoo, S. Menzel, C. Funck, F. Cueppers, D. J. Wouters, C. S. Hwang, R. Waser, S. Hoffmann-Eifert, *ACS Appl. Mater. Interfaces* **2018**, *10*, 29766.
[21] L. Goux, Y. Chen, L. Pantisano, X. Wang, G. Groeseneken, M. Jurczak, D. J. Wouters, *Electrochem. Solid-State Lett.* **2010**, *13*, G54.
[22] K.-C. Liu, K.-C. Liu, K.-M. Chang, C.-H. Wu, *Surf. Coat. Technol.* **2010**, *205*, 379.
[23] M. Moors, K. K. Adepalli, Q. Lu, A. Wedig, C. Bäumer, K. Skaja, B. Arndt, H. L. Tuller, R. Dittmann, R. Waser, B. Yildiz, I. Valov, *ACS Nano* **2016**, *10*, 1481.
[24] A. Schönhals, C. M. M. Rosario, S. Hoffmann-Eifert, R. Waser, S. Menzel, D. J. Wouters, *Adv. Electron. Mater.* **2018**, *4*, 1700243.
[25] R. Muenstermann, T. Menke, R. Dittmann, R. Waser, *Adv. Mater.* **2010**, *22*, 4819.
[26] S. A. Mojarad, J. P. Goss, K. S. K. Kwa, P. K. Petrov, B. Zou, N. Alford, A. O'Neill, *J. Appl. Phys.* **2012**, *112*, 124516.
[27] S. Ambrogio, S. Balatti, V. Milo, R. Carboni, Z. Wang, A. Calderoni, N. Ramaswamy, D. Ielmini, *IEEE Trans. Electron Devices* **2016**, *63*, 1508.
[28] G. W. Burr, R. M. Shelby, A. Sebastian, S. Kim, S. Kim, S. Sidler, K. Virwani, M. Ishii, P. Narayanan, A. Fumarola, L. L. Sanches, I. Boybat, M. L.e Gallo, K. Moon, J. Woo, H. Hwang, Y. Leblebici, *Adv. Phys.: X* **2017**, *2*, 89.
[29] H. Wu, P. Yao, B. Gao, W. Wu, Q. Zhang, W. Zhang, N. Deng, D. Wu, H.-S. P. Wong, S. Yu, H.e Qian, IEEE International Electron Devices Meeting (IEDM) 2017 **2017**.
[30] J. Xiong, R. Yang, J. Shaibo, H. M. Huang, H. K. He, W. Zhou, X. Guo, *Adv. Funct. Mater.* **2019**, *29*, 1807316.
[31] T. Heisig, C. Baeumer, U. N. Gries, M. P. Mueller, C. La Torre, M. Luebben, N. Raab, H. Du, S. Menzel, D. N. Mueller, C.-L. Jia, J. Mayer, R. Waser, I. Valov, R. A. De Souza, R. Dittmann, *Adv. Mater.* **2018**, *30*, 1800957.
[32] C. Baeumer, C. Schmitz, A. H. H. Ramadan, H. Du, K. Skaja, V. Feyer, P. Muller, B. Arndt, C. Jia, J. Mayer, R. A. De Souza, C. M. Schneider, R. Waser, R. Dittmann, *Nat. Commun.* **2015**, *6*, 9610.
[33] J. Woo, K. Moon, J. Song, S. Lee, M. Kwak, J. Park, H. Hwang, *IEEE Electron Device Lett.* **2016**, *37*, 994.
[34] H. Y. Lee, P. S. Chen, T. Y. Wu, Y. S. Chen, C. C. Wang, P. J. Tzeng, C. H. Lin, F. Chen, C. H. Lien, M.-J. Tsai, *IEEE Trans. Dielectr. Electr. Insul.* **2008**, 1.
[35] S. Lee, Y. Kim, M. Chang, K. Kim, C. Lee, J. Hur, G. Park, D. Lee, M. Lee, C. Kim, U. Chung, I. Yoo, K. Kim, *Digest of Technical Papers – Symposium on VLSI Technology* **2012**, 151.
[36] D. Gilmer, G. Bersuker, H. Park, C. Park, B. Butcher, W. Wang, P. Kirsch, R. Jammy, *IMW* **2011**, 5873225.
[37] C. Xu, M. Moors, R. Dittmann, *Appl. Surf. Sci.* **2015**, *359*, 68.
[38] F. V. E. Hensling, T. Heisig, N. Raab, C. Baeumer, R. Dittmann, *Solid State Ionics* **2018**, *325*, 247.
[39] T. Tsuruoka, K. Terabe, T. Hasegawa, M. Aono, *Nanotechnology* **2011**, *22*, 254013.
[40] S. Menzel, M. Waters, A. Marchewka, U. Böttger, R. Dittmann, R. Waser, *Adv. Funct. Mater.* **2011**, *21*, 4487.
[41] Y. Nishi, S. Menzel, K. Fleck, U. Boettger, R. Waser, *IEEE Electron Device Lett.* **2013**, *35*, 259.
[42] S. Larentis, F. Nardi, S. Balatti, D. C. Gilmer, D. Ielmini, *IEEE Trans. Electron Devices* **2012**, *59*, 2468.
[43] S. Menzel, U. Böttger, M. Wimmer, M. Salinga, *Adv. Funct. Mater.* **2015**, *25*, 6306.
[44] R. Merkle, J. Maier, *Angew. Chem., Int. Ed.* **2008**, *47*, 3874.
[45] R. Merkle, J. Maier, *Phys. Chem. Chem. Phys.* **2002**, *4*, 4140.
[46] J. O.´M. Bockris, A. K. N. Reddy, M. Gamboa-Aldeco, *Modern Electrochemistry 2A. Fundamentals of Electrodics*, Kluwer Academic/Plenum Publishers, Dordrecht, Netherlands **2000**.
[47] D. A. Noren, M. A. Hoffmann, *J. Power Sources* **2005**, *152*, 175.
[48] C. Baeumer, C. Schmitz, A. Marchewka, D. N. Mueller, R. Valenta, J. Hackl, N. Raab, S. P. Rogers, M. I. Khan, S. Nemsak, M. Shim, S. Menzel, C. M. Schneider, R. Waser, R. Dittmann, *Nat. Commun.* **2016**, *7*, 12398.
[49] A. R. Genreith-Schriever, R. A. De Souza, *Phys. Rev. B: Condens. Matter Mater. Phys.* **2016**, *94*, 224304.
[50] S. Menzel, K. Fleck, Y. Nishi, S. Tappertzhofen, J. van den Hurk, B. Rösgen, A. Marchewka, V. Rana, I. Valov, U. Böttger, R. Waser, *N. Days* **2015**.
[51] L. Wang, R. Merkle, Y. A. Mastrikov, E. A. Kotomin, J. Maier, *J. Mater. Res.* **2012**, *27*, 2000.
[52] T. Yonekura, Y. Tachikawa, T. Yoshizumi, Y. Shiratori, K. Ito, K. Sasaki, *ECS Trans.* **2011**, *35*, 1007.
[53] R. Schmiedl, V. Demuth, P. Lahnor, H. Godehardt, Y. Bodschwinna, C. Harder, L. Hammer, H. P. Strunk, M. Schulz, K. Heinz, *Appl. Phys. A* **1996**, *62*, 223.
[54] R. Stumpf, C. Liu, C. Tracy, *Phys. Rev. B: Condens. Matter Mater. Phys.* **1999**, *59*, 16047.
[55] E. Mutoro, C. Hellwig, B. Luerssen, S. Guenther, W. G. Bessler, J. Janek, *Phys. Chem. Chem. Phys.* **2011**, *13*, 12798.
[56] X. R. Wang, X. Xiao, Z. Zhang, *Surf. Sci.* **2002**, *512*, L361.
[57] L. R. Velho, R. W. Bartlett, *Metall. Trans.* **1972**, *3*, 65.
[58] T. K. Sherwood, R. L. Pigford, C. R. Wilke, *Mass Transfer*, MacGraw Hill, New York **1975**.
[59] T. Nabatame, T. Yasuda, M. Nishizawa, M. Ikeda, T. Horikawa, A. Toriumi, *Jpn. J. Appl. Phys.* **2003**, *42*, 7205.
[60] S. Stathopoulos, A. Khiat, M. Trapatseli, S. Cortese, A. Serb, I. Valov, T. Prodromakis, *Sci. Rep.* **2017**, *7*, 17532.

[61] C. Ye, T. Deng, J. Zhang, L. Shen, P. He, W. Wei, H. Wang, *Semicond. Sci. Technol.* **2016**, *31*, 105005.
[62] B. Hudec, A. Paskaleva, P. Jancovic, J. Derer, J. Fedor, A. Rosova, E. Dobrocka, K. Froehlich, *Thin Solid Films* **2014**, *563*, 10.
[63] C. T. Chou, B. Hudec, C. W. Hsu, W. L. Lai, C. C. Chang, T. H. Hou, *Microelectron. Reliab.* **2015**, *55*, 2220.
[64] R. Merkle, J. Maier, *Angew. Chem., Int. Ed.* **2008**, *47*, 3874.
[65] Z. Guo, F. Ambrosio, A. Pasquarello, *Appl. Phys. Lett.* **2016**, *100*, 1.
[66] R. Waser, *J. Am. Ceram. Soc.* **1991**, *74*, 1934.
[67] Y. Oishi, K. Ando, Y. Kubota, *J. Chem. Phys.* **1980**, *73*, 1410.
[68] M. Schmidbauer, A. Kwasniewski, J. Schwarzkopf, *Acta Crystallogr., Sect. B: Struct. Sci., Cryst. Eng. Mater.* **2012**, *68*, 8.
[69] R. Takahashi, Y. Matsumoto, T. Ohsawa, M. Lippmaa, M. Kawasaki, H. Koinuma, *J. Cryst. Growth* **2002**, *234*, 505.
[70] W. Martienssen, H. Warlimont, *Springer Handbook of Condensed Matter and Materials Data*, Springer, Berlin Heidelberg **2005**.
[71] C. Funck, S. Menzel, *AIP Adv.* **2019**, *9*, 045116.
[72] K. PF, *Properties of Materials*, Taylor & Francis Group, New Delhi **2014**.
[73] H. Szelagowski, I. Arvanitides, S. Seetharaman, *J. Appl. Phys.* **1999**, *85*, 193.
[74] I. Stark, M. Stordeur, F. S., *Thin Solid Films* **1993**, *226*, 185.
[75] D. deLigny, P. Richet, *Phys. Rev. B* **1996**, *53*, 3013.
[76] C. T. Anderson, *J. Am. Chem. Soc.* **1935**, *57*, 429.